IEEE Access
Multidisciplinary | Rapid Review | Open Access Journal

Received 27 January 2023, accepted 13 February 2023, date of publication 21 February 2023, date of current version 27 February 2023.

Digital Object Identifier 10.1109/ACCESS.2023.3246503

RESEARCH ARTICLE

Anomalous Reflection From a Phase Gradient Metasurface With Arbitrary Incident Angle

WIHAN BARNARD, JOHANN W. ODENDAAL, (Senior Member, IEEE), AND JOHAN JOUBERT, (Senior Member, IEEE)

Centre for Electromagnetism, Department of Electrical, Electronic and Computer Engineering, University of Pretoria, Pretoria 0002, South Africa

Corresponding author: Johann W. Odendaal (wimpie.odendaal@up.ac.za)

ABSTRACT A planar phase gradient metasurface (PGM) with phase gradients in two in-plane directions will introduce two additional wave vectors to the reflected wave vector. For small incident angles, close to the normal vector, the magnitude of the reflected wave vector is smaller than that of the incident wave vector and the direction of the anomalous reflected wave can be determined from the incident wave vector components and additional phase gradient components. The expanded generalized Snell's law, which includes diffraction order modes, is combined with array theory to accurately predict the directions of the reflected waves from a planar PGM for incident angles where the magnitude of the reflected wave vector is larger than that of the incident wave vector. The predicted directions of the reflected waves from a planar PGM are compared with simulated RCS results obtained with CST Studio Suite and measured results obtained in a compact range.

INDEX TERMS Bistatic radar, electromagnetic metamaterials, electromagnetic reflection, radar cross-sections.

I. INTRODUCTION

Phase gradient metasurfaces (PGMs) are used to manipulate the radar cross section (RCS) of planar structures for monostatic and bistatic RCS applications [1], [2], [3]. PGMs can be designed to reduce or enhance the RCS of structures for specific scenarios if it is possible to predict the directions of the reflected waves from the PGM for arbitrary incident angles. The direction of the anomalous reflected wave is determined from the incident wave vector components and additional phase gradient components of the PGM. Predicting the directions of the scattered waves from PGMs with dual gradients are currently restricted to perpendicular incidence [4] or small incident angles close to the normal vector [5], [6]. These restrictions are limiting the application of PGMs for RCS control to scenarios where the incident angle is smaller than the critical value [7], i.e. when the summation of the reflected wave vector, due to the incident angle, and the phase gradient vector do not exceed the magnitude of the initial incident wave vector. In [8] a PGM was used to control the scattering direction of optical waves. In [9] a general method is proposed to control the diffraction pattern both in angle and energy ratio between the scattered beams. This proposed method only consider scattered beams with incident angles smaller than the critical value. In [4], [7], and [8] it is claimed that incident angles smaller than the critical value cause anomalous reflected waves and incident angles larger than the critical value cause non-radiating surface waves.

In [10] it was shown that incident angles larger than the critical value are converted to evanescent surface waves. The phenomenon of negative reflection was also introduced in [10] for acoustic waves. A generalized Snell's law of reflection was formulated that depends on the incident and reflected wave vectors. This formulation makes it possible to predict the directions of the reflected waves from a PGM for scenarios where the incident wave angle is larger than the critical value. Subsequently the bistatic RCS of a PGM with a one dimensional phase gradient was considered and multiple directions for reflected modes were estimated in [11]. However, full wave scattering simulations of PGMs using CST Studio Suite [12] show additional reflected energy, close to

The associate editor coordinating the review of this manuscript and approving it for publication was Fulvio Schettino.

the plane of the PGM at $\theta_r = 90°$, not predicted by any of the valid diffraction order modes.

In [13] the angular directions of the scattered waves for a checkerboard metasurface were determined using array theory with inspiration from [14].

Destructive interference was utilized in [15] to design a surface, utilizing artificial magnetic conductor (AMC) elements, which reflect the incident wave simultaneously in phase and out of phase. The idea behind this concept is explained using array theory by modelling the unit cell as a 2 × 2 antenna array consisting of 4 antenna elements (representing the two different AMC elements) and assuming (as a first order approximation) that the four antennas all radiate the same amount of power.

In this paper the generalized Snell's law of reflection from [10] and [11] is extended to account for PGMs with different phase gradients in two orthogonal in-plane directions. The extended formulation is combined with antenna array theory concepts [13], [15] to estimate the finite number of scattering modes and accurately estimate the directions of the reflected waves. The formulation also takes into account the scattering beamwidth of the reflected waves from a finite PGM to estimate the directions of reflected waves close to the plane of the PGM. The estimated directions of the reflected waves from a planar PGM are compared with simulated RCS results obtained with CST Studio Suite, and measured results obtained in a compact range.

II. PROBLEM FORMULATION

A. GENERALISED SNELL'S LAW OF REFLECTION

The directions of the reflected waves from a PGM with phase gradients in two orthogonal in-plane directions are illustrated in Fig. 1. The relationship between the incident wave direction and reflected wave directions for incident angles smaller than the critical value is described by Snell's law of reflection [4], [5], [6], [7], [8]. The direction of the specular reflected wave, θ_r and φ_r, is expressed in [6] as

$$\theta_r = arcsin\left(\frac{\sqrt{(\nabla\phi_x + k_{ix})^2 + \left(\nabla\phi_y + k_{iy}\right)^2}}{k_i}\right)$$
$$\varphi_r = arctan\left(\frac{k_{iy} + \nabla\phi_y}{k_{ix} + \nabla\phi_x}\right), \quad (1)$$

with k_{ix} and k_{iy} the magnitudes of the in-plane vector components of the incident wave vector, $\mathbf{k_i}$. $\nabla\phi_x$ and $\nabla\phi_y$ are the orthogonal phase gradients of the PGM along the x- and y-direction, respectively. If the incident angle is larger than the critical value, the numerator in (1) exceeds the denominator, and θ_r results in a complex value, and according to [6] the incident wave is coupled into a surface wave.

In [11] a PGM with a one dimensional phase gradient is considered and Snell's law is extended to incident angles larger than the critical value using a diffraction order element,

$$sin\theta_r - sin\theta_i = \frac{1}{\beta}\sigma\nabla\phi(1 + \eta_G), \quad (2)$$

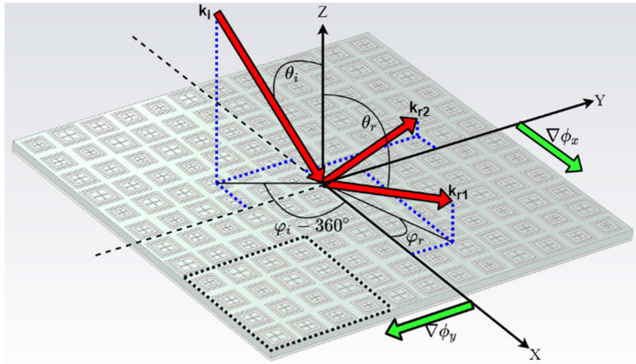

FIGURE 1. A reflective PGM with phase gradients in two orthogonal in-plane directions, illustrating the incident and reflected wave vectors as well as phase gradient vectors. The dashed square indicates a sub cell consisting of 4 × 4 AMC elements.

where β is the wavenumber of the incident wave, $\nabla\phi$ is the phase gradient of the PGM, η_G is the diffraction order, and $\sigma = 1$ or $\sigma = -1$ a parameter indicating the direction of the phase gradient.

For a PGM with phase gradients in two orthogonal in-plane directions and an incident wave from an arbitrary direction, (θ_i, φ_i), (2) can be rewritten as

$$\beta sin\theta_r cos\varphi_r = \beta sin\theta_i cos(\varphi_i - \pi) + \sigma\nabla\phi_x(1 + \eta_G)$$
$$\beta sin\theta_r sin\varphi_r = \beta sin\theta_i sin\left(\varphi_i - \pi\right) + \sigma\nabla\phi_y\left(1 + \eta_G\right). \quad (3)$$

$\nabla\phi_x$ and $\nabla\phi_y$ are the phase gradients of the PGM in the x- and y-direction, respectively. The directions of reflected waves, θ_r, φ_r, are determined by simultaneously solving (3) for different diffraction order values, η_G. Valid diffraction order modes will result in real values for the directions of the reflected waves [11]. However, full wave CST Studio Suite scattering simulations of PGMs show additional reflected energy, close to the plane of the PGM that is not predicted by any of the valid diffraction order modes [16].

B. ANTENNA ARRAY THEORY AND SCATTERING FROM A PGM

Snell's law describes the relationship between the angle of incidence and reflection for a wave incident on an infinite surface. Practical PGMs are finite in size and will produce a reflected wave with a finite beamwidth, rather than a plane wave in a single direction [17].

A PGM is designed using AMC elements, which provide a uniform amplitude reflection and varied phase reflection. This phase reflection is controlled by varying certain parameters of the AMC elements [4]. Fig. 1 shows a reflective PGM consisting of 3 × 3 sub cells and 4 × 4 AMC elements per sub cell, realizing phase gradients in two orthogonal in-plane directions.

Following [1], [13], [14], [15] the scattering from the PGM can be analyzed as an equally spaced uniformly excited planar array. The normalized array factor for uniformly excited and equally spaced planar arrays [17], adapted to the scattering

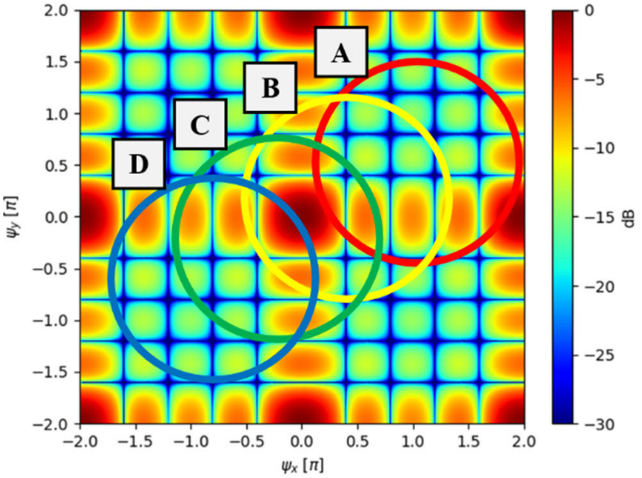

FIGURE 2. Normalized array factor, $f_{xy}\left(\psi_x, \psi_y\right)$ with visible space regions indicated by various ellipses.

from a PGM for an incident wave from an arbitrary direction (θ_i, φ_i) is

$$f_{xy}(\theta,\varphi)=\left|\frac{sin\left(\frac{N\psi_x(\theta,\varphi)}{2}\right)}{Nsin\left(\frac{\psi_x(\theta,\varphi)}{2}\right)}\times\frac{sin\left(\frac{N\psi_y(\theta,\varphi)}{2}\right)}{Nsin\left(\frac{\psi_y(\theta,\varphi)}{2}\right)}\right|, \quad (4)$$

with

$$\begin{aligned}\psi_x(\theta,\varphi) &= \beta d_x\left(sin\theta cos\varphi - sin\theta_i cos(\varphi_i-\pi)\right)\\ &\quad +\sigma\nabla\phi_x d_x(1+\eta_G)\\ \psi_y(\theta,\varphi) &= \beta d_y\left(sin\theta sin\varphi - sin\theta_i sin(\varphi_i-\pi)\right)\\ &\quad +\sigma\nabla\phi_y d_y(1+\eta_G) \end{aligned}\quad (5)$$

where $N \times N$ represents the number of AMC elements in one sub cell; β is the wavenumber of the incident wave and (d_x, d_y) the spacing between the center points of the AMC elements in the x- and y-direction, respectively.

The normalized array factor, $f_{xy}(\psi_x, \psi_y)$, for a sub cell with 4×4 AMC elements is shown in Fig. 2. The visible space regions [17] are given for different diffraction orders, η_G by

$$\frac{(\psi_x-\psi_x(0,0))^2}{(\beta d_x)^2}-\frac{\left(\psi_y-\psi_y(0,0)\right)^2}{\left(\beta d_y\right)^2}=1 \quad (6)$$

and correspond with ellipses A, B, C and D for diffraction order values, $\eta_G = 0, -1, -2,$ and -3, respectively. The peak in the visible space regions B and C corresponds to valid diffraction order modes due to higher order diffraction values, $\eta_G = -1$ and $\eta_G = -2$, respectively. The directions of these two reflected waves, determined using (3) will result in real values for the directions of the reflected waves.

The visible space regions A and D contain no peaks and correspond with non-valid diffraction order values; (3) will return imaginary values for θ_r and no reflected waves are expected. Although there is no peak in ellipse D, a significant portion of the ellipse intersects with at least half of the peak at the center of the normalized array factor and will result in reflected energy close to the plane of the PGM. The analogy of this reflected wave to array theory is that at least -3 dB of the grating lobe appears in the visible space [17].

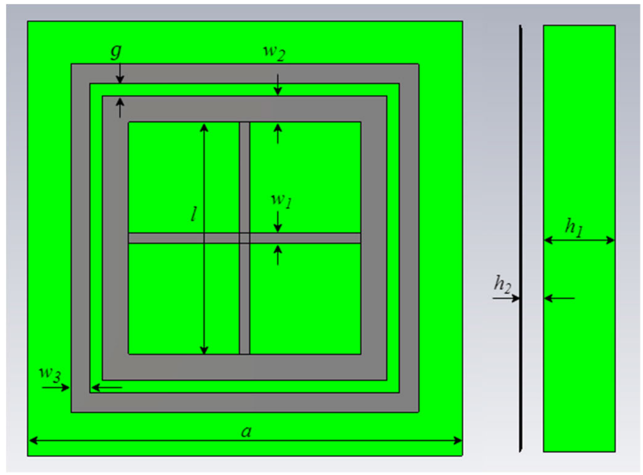

(a) (b)

FIGURE 3. Geometry of the AMC element. (a) Top view. (b) Side view.

TABLE 1. Parameters of simulated AMC elements.

Symbol	Description	Value (mm)
a	width of AMC element	12
w_1	width of cross	0.4
w_2	width inner square ring	1.1
w_3	width outer square ring	0.8
g	gap between the rings	0.5
l	length of cross (for the 4 elements, respectively)	3.4, 4.2, 4.7, 5.6
h_1	height of substrate	3
h_2	air gap between substrate and ground plane	1

III. SIMULATED RESULTS

The estimated directions of the reflected waves from a planar PGM are compared with simulated RCS results obtained with CST Studio Suite. Detailed design information for PGMs can be found in [4] and [18]. The AMC element from [4] was implemented on Rogers 5880 substrate to realize a sub cell consisting of 4×4 AMC elements. The parameters of the AMC elements are defined in Fig. 3 and Table 1.

The parameter l is used to control the phase reflection of the unit cell. The phase differences between adjacent AMC elements, were designed as $\delta\phi_x = \pi/2$ rad and $\delta\phi_y = \pi/2$ rad at 10 GHz. The phase gradient of the PGM is the change in phase over the width of the AMC element,

$$\nabla\phi_{x,y}=\frac{\delta\phi_{x,y}}{a}. \quad (7)$$

In [4] a detailed PGM design procedure is provided which was utilized to design the simulated and manufactured PGMs in this paper. The layout of the AMC elements realizing a

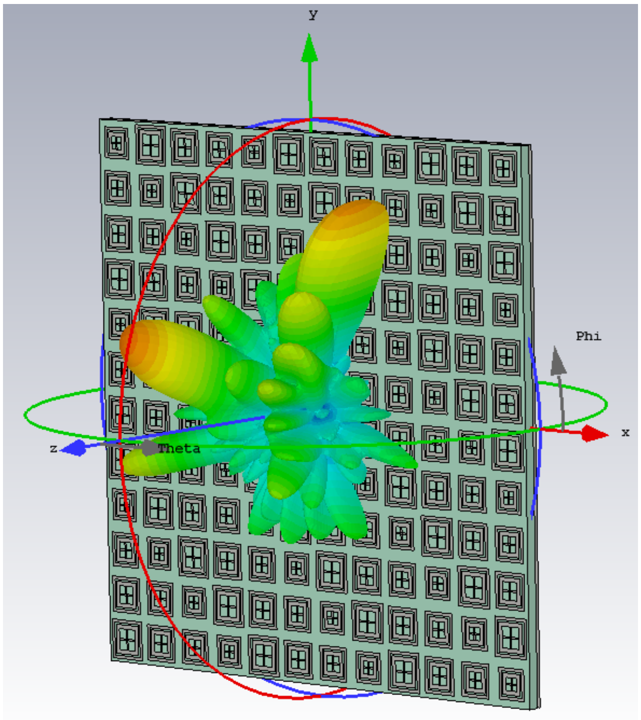

FIGURE 4. A 3-D scattering pattern for incident plane wave at $\theta_i = 60^\circ, \varphi_i = 20^\circ$.

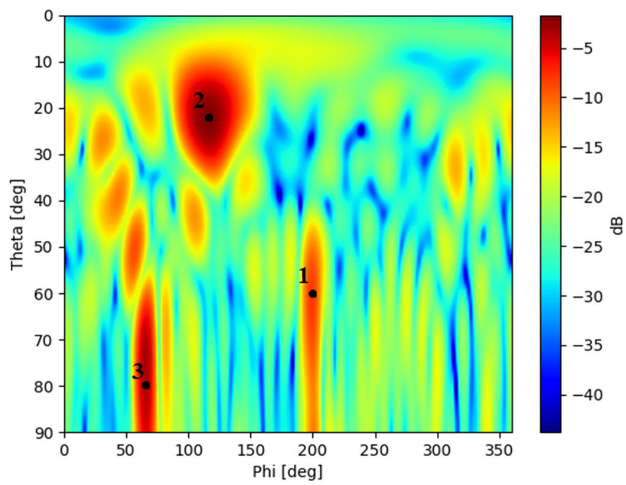

FIGURE 5. Bistatic scattering from PGM, illustrating the directions of reflected waves.

3×3 PGM and simulated bistatic RCS results for an incident plane wave at $\theta_i = 60^\circ, \varphi_i = 20^\circ$ are shown in Figs. 4 and 5. There are three distinct scattering directions at approximately $(\theta_1 = 60^\circ, \varphi_1 = 200^\circ)$, $(\theta_2 = 22^\circ, \varphi_2 = 115^\circ)$ and $(\theta_3 = 80^\circ, \varphi_3 = 65^\circ)$.

The predicted directions of the reflected waves using (3) for an incident plane wave from $\theta_i = 60^\circ, \varphi_i = 20^\circ$ are given in Table 2. Two valid diffraction orders produce real directions for reflected waves viz. $\eta_G = -1$ and $\eta_G = -2$ corresponding to directions of reflected waves

TABLE 2. Calculated results for various diffraction orders.

Diffraction Order, η_G	θ_r (°)	φ_r (°)
1	90– j109	216.6
0	90 – j64.7	212.6
-1	60	200
-2	22.3	119.9
-3	90 – j17.8	65.3

TABLE 3. Parameters of measured AMC elements.

Symbol	Description	Value (mm)
a	width of AMC element	24
w_1	width of cross	0.8
w_2	width inner square ring	1.1
w_3	width outer square ring	1.6
g	gap between the rings	1.0
l	length of cross (for the 4 elements, respectively)	6.0, 7.6, 8.1, 9.2
h_1	height of substrate	6.4
h_2	air gap between substrate and ground plane	0.0

at $(\theta_1 = 60^\circ, \varphi_1 = 200^\circ)$ and $(\theta_2 = 22.3^\circ, \varphi_2 = 119.9^\circ)$, respectively.

The visible space regions A, $(\eta_G = 0)$ and D, $(\eta_G = -3)$ in Fig. 2 contain no peaks and correspond with non-valid diffraction order values; (3) returned complex values for θ_r and no reflected waves are expected. A significant portion of ellipse D intersects with at least half of the peak at the center of the normalized array factor and resulted in a predicted reflected wave close to the plane of the PGM $(\theta_3 = 90^\circ)$ at $\varphi_3 = 65.3^\circ$. The predicted directions for the reflected waves correspond very closely to that observed in the CST simulation, as seen in Fig. 5. The slight difference in predicted value for θ_3 can be attributed to edge diffraction due to the finite size of the simulated PGM.

IV. MEASURED RESULTS

Monostatic RCS measurements were performed in the compact range at the University of Pretoria and compared to simulated RCS results using CST Studio Suite. The PGM used in these measurements was designed with CST Studio Suite to operate at 5 GHz, using FR-4 substrate with no air gap between the substrate and ground plane. Four AMC elements were designed with a phase difference of $\delta\phi_x = \pi/2$ rad and $\delta\phi_y = 0$ rad, the parameters are defined in Table 3.

The manufactured PGM is shown in Fig. 6. The monostatic RCS measurement setup in the compact range is shown in Fig. 7. The PGM is mounted on a polystyrene column allowing azimuth rotation in the quiet zone of the compact range and the offset parabolic reflector is used for transmit and receive. The azimuth angle of the PGM relative to the parabolic reflector corresponds to the incident angle, θ_i, and for monostatic RCS also to the reflected angle, θ_r. Because the incident angle is equal to the reflected angle for

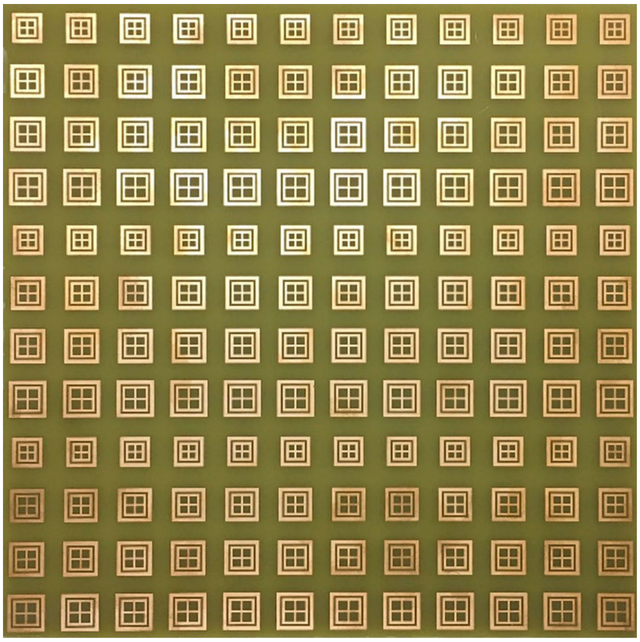

FIGURE 6. PGM prototype measured in the compact range.

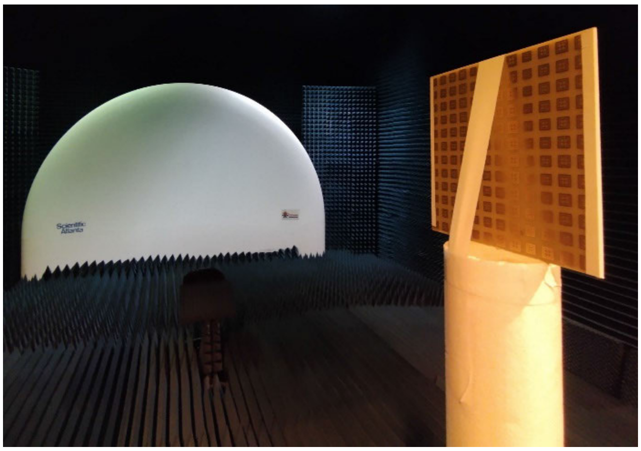

FIGURE 7. Setup for monostatic RCS measurement in the compact range.

TABLE 4. Directions of reflected waves for monostatic RCS results.

Diffraction Order, η_G	Measured (θ_r, φ_r) (°)	Calculated (θ_r, φ_r) (°)
-2	(18, 0)	(18.4, 0)
1	(38, 180)	(37.9, 180)
2	(69, 180)	(70.3, 180)

monostatic RCS measurements, only reflected waves with reflection angles equal to incident angles will be observed in the RCS measurement of the PGM.

The results of the monostatic RCS measurement and CST simulation are shown in Fig 8 and summarized in Table 4. The slight difference between the measured and simulated RCS values is probably due to alignment of the PGM in the compact range. Three distinct peaks are observed at approximately $\theta_{r1} = 18°, \theta_{r2} = -38°$ and $\theta_{r3} = -69°$ in the

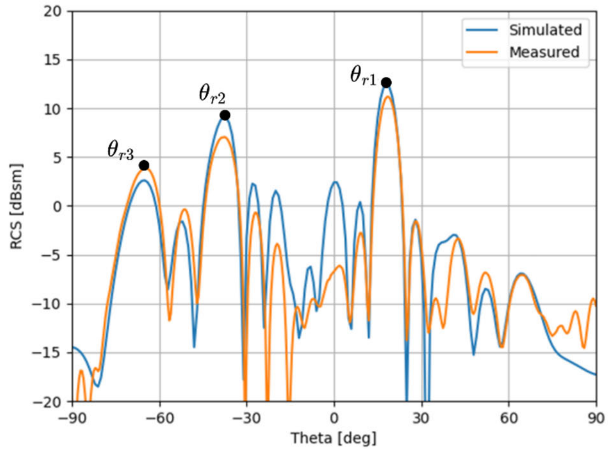

FIGURE 8. Monostatic RCS measured and simulated results.

measured and simulated results and represent the directions of the reflected waves. Using the formulation in Section II and taking into account that for monostatic RCS measurements the incident angle is equal to the reflected angle, the direction of the first reflected wave was estimated as $\theta_{r1} = 18.4°$ for a diffraction order $\eta_G = -2$. The direction of the second reflected wave was estimated as $\theta_{r2} = -37.9°$, for a diffraction order, $\eta_G = 1$, and the direction of the third reflected wave was estimated as $\theta_{r3} = -70.3°$, corresponding to a diffraction order $\eta_G = 2$.

V. CONCLUSION

A planar PGM with phase gradients in two in-plane directions will introduce two additional wave vectors to the reflected wave vector. For small incident angles, close to the normal vector, the magnitude of the reflected wave vector is smaller than that of the incident wave vector and the direction of the anomalous reflected wave can be determined from the incident wave vector components and additional phase gradient components.

The generalized Snell's law of reflection presented in [10], made it possible to predict the directions of reflected waves from PGMs for incident angles larger than the critical value. In this paper, the generalized Snell's law of reflection was extended to account for PGMs with different orthogonal phase gradients in the two in-plane directions. The extended formulation is used to predict all the scattering modes and to accurately estimate the directions of the reflected waves. The extended formulation is combined with antenna array theory concepts to account for the scattering beamwidth of reflected waves close to the plane of a finite PGM.

The estimated directions of the reflected waves from a planar PGM were compared with simulated RCS results obtained with CST Studio Suite and measured results.

REFERENCES

[1] A. Y. Modi, M. A. Alyahya, C. A. Balanis, and C. R. Birtcher, "Metasurface-based method for broadband RCS reduction of dihedral corner reflectors with multiple bounces," *IEEE Trans. Antennas Propag.*, vol. 68, no. 3, pp. 1436–1447, Mar. 2020.

[2] Y. Yuan, K. Zhang, B. Ratni, Q. Song, X. Ding, Q. Wu, S. N. Burokur, and P. Genevet, "Independent phase modulation for quadruplex polarization channels enabled by chirality-assisted geometric-phase metasurfaces," *Nature Commun.*, vol. 11, no. 1, p. 4186, Aug. 2020.

[3] M. K. T. Al-Nuaimi, G.-L. Huang, W. G. Whittow, D. Wang, R.-S. Chen, S.-W. Wong, and K.-W. Tam, "Coding engineered reflector for wide-band RCS reduction under wide angle of incidence," *IEEE Trans. Antennas Propag.*, vol. 70, no. 10, pp. 9947–9952, Oct. 2022.

[4] W. Zhang, Y. Liu, S. Gong, J. Wang, and Y. Jiang, "Wideband RCS reduction of a slot array antenna using phase gradient metasurface," *IEEE Antennas Wireless Propag. Lett.*, vol. 17, no. 12, pp. 2193–2197, Dec. 2018.

[5] F. Yuan, G.-M. Wang, H.-X. Xu, T. Cai, X.-J. Zou, and Z.-H. Pang, "Broadband RCS reduction based on spiral-coded metasurface," *IEEE Antennas Wireless Propag. Lett.*, vol. 16, pp. 3188–3191, 2017.

[6] Y. Li, J. Zhang, S. Qu, J. Wang, H. Chen, Z. Xu, and A. Zhang, "Wideband radar cross section reduction using two-dimensional phase gradient metasurfaces," *Appl. Phys. Lett.*, vol. 104, no. 22, Jun. 2014, Art. no. 221110.

[7] S. Sun, Q. He, S. Xiao, Q. Xu, X. Li, and L. Zhou, "Gradient-index metasurfaces as a bridge linking propagating waves and surface waves," *Nature Mater.*, vol. 11, no. 5, pp. 426–431, 2012.

[8] N. Yu, P. Genevet, M. A. Kats, F. Aieta, J.-P. Tetienne, F. Capasso, and Z. Gaburro, "Light propagation with phase discontinuities: Generalized laws of reflection and refraction," *Science*, vol. 334, no. 6054, pp. 333–337, Oct. 2011.

[9] Y. Wang, Y. Yuan, G. Yang, X. Ding, Q. Wu, Y. Jiang, S. N. Burokur, and K. Zhang, "Perfect control of diffraction patterns with phase-gradient metasurfaces," *ACS Appl. Mater. Interfaces*, vol. 14, no. 14, pp. 16856–16865, Apr. 2022.

[10] Y. Xie, W. Wang, H. Chen, A. Konneker, B.-I. Popa, and S. A. Cummer, "Wavefront modulation and subwavelength diffractive acoustics with an acoustic metasurface," *Nature Commun.*, vol. 5, no. 1, p. 5553, Nov. 2014.

[11] X. Ding, C. Guan, Z. Wang, S. Liu, K. Zhang, X. Gu, Q. Wu, and M. Jin, "Metasurface for bending the reflected wave under oblique incidence," *IEEE Trans. Magn.*, vol. 55, no. 11, pp. 1–4, Nov. 2019, Art. no. 7502804.

[12] *CST Studio Suite Electromagnetic Field Simulation Software*. Dassault Systèmes, Vélizy-Villacoublay, France, 2021.

[13] A. Y. Modi, C. A. Balanis, C. R. Birtcher, and H. N. Shaman, "Novel design of ultrabroadband radar cross section reduction surfaces using artificial magnetic conductors," *IEEE Trans. Antennas Propag.*, vol. 65, no. 10, pp. 5406–5417, Jul. 2017.

[14] J. C. I. Galarregui, A. T. Pereda, J. L. M. De Falcón, I. Ederra, R. Gonzalo, and P. De Maagt, "Broadband radar cross-section reduction using AMC technology," *IEEE Trans. Antennas Propag.*, vol. 61, no. 12, pp. 6136–6143, Dec. 2013.

[15] M. Paquay, J. C. Iriarte, I. Ederra, R. Gonzalo, and P. D. Maagt, "Thin AMC structure for radar cross-section reduction," *IEEE Trans. Antennas Propag.*, vol. 55, no. 12, pp. 3630–3638, Dec. 2007.

[16] W. Barnard, J. W. Odendaal, and J. Joubert, "Predicting the direction of the reflected wave from a phase gradient metasurface with arbitrary incident angle," presented at the IEEE Int. Symp. Antennas Propag. USNC-URSI Radio Sci. Meeting, Singapore, Dec. 2021.

[17] W. L. Stutzman and G. A. Thiele, "Array antennas," in *Antenna Theory and Design*. 3rd ed. Hoboken, NJ, USA: Wiley, 2013, pp. 275–280.

[18] B. Lin, J. Guo, L. Lv, Z. Liu, X. Ji, and J. Wu, "An ultra-wideband reflective phase gradient metasurface using Pancharatnam–Berry phase," *IEEE Access*, vol. 7, pp. 13317–13325, 2019.

WIHAN BARNARD received the B.Eng. degree in electronic engineering from the University of Pretoria, Pretoria, South Africa, in 2017. He has been working in the EMF safety industry, since 2018, writing simulation software used by major telecommunication companies to design antenna sites as safe as possible. His research interests include electromagnetic scattering and radiation and RCS reduction with metamaterials and antenna arrays.

JOHANN W. ODENDAAL (Senior Member, IEEE) received the B.Eng., M.Eng., and Ph.D. degrees in electronic engineering from the University of Pretoria, Pretoria, South Africa, in 1989, 1991, and 1994, respectively.

From September 1993 to April 1994, he was a Visiting Scientist with the ElectroScience Laboratory, The Ohio State University. From August 2002 to December 2002, he was a Visiting Scientist with CSIRO Telecommunications and Industrial Physics, Australia. Since May 1994, he has been with the University of Pretoria, where he is currently a Full Professor. He is also the Director of the Centre for Electromagnetism, University of Pretoria. His research interests include electromagnetic scattering and radiation, compact range measurements, and signal processing.

Prof. Odendaal is a member of the Antenna Measurement Techniques Association (AMTA) and registered as a Professional Engineer in South Africa.

JOHAN JOUBERT (Senior Member, IEEE) received the B.Eng., M.Eng., and Ph.D. degrees in electronic engineering from the University of Pretoria, Pretoria, South Africa, in 1983, 1987, and 1991, respectively.

From 1984 to 1988, he was employed as a Research Engineer with the Council for Scientific and Industrial Research, Pretoria. In 1988, he joined the Department of Electrical and Electronic Engineering, University of Pretoria, where he is currently a Professor of electromagnetism. From July 1995 to December 1995, he was a Visiting Scholar with the Department of Electrical and Computer Engineering, California State University, Northridge, CA, USA. From July 2001 to December 2001, he was a Visiting Scientist with Industrial Research Laboratories, Wellington, New Zealand. From July 2006 to December 2006, he was a Visiting Scholar with the Institut für Höchstfrequenztechnik und Elektronik, Universität Karlsruhe (TH), Germany. From July to September 2010, he visited Loughborough University, U.K., for a collaborative research project on metamaterials. His research interests include antenna array design and computational electromagnetism.

Prof. Joubert is a registered Professional Engineer in South Africa.